Wettability of non-metallic inclusions and its impact on bubble-induced flotation kinetics

Falsetti, Luís Otávio Z.; Delfos, René; Charruault, Florian; Luchini, Bruno; Van Der Plas, Dirk; Pandolfelli, Victor C.

DOI
10.1111/ijac.14849

Publication date
2024

Document Version
Final published version

Published in
International Journal of Applied Ceramic Technology

Received: 8 February 2024 | Revised: 21 May 2024 | Accepted: 3 June 2024

DOI: 10.1111/ijac.14849

International Journal of Applied Ceramic Technology

RAPID COMMUNICATION

Wettability of non-metallic inclusions and its impact on bubble-induced flotation kinetics

Luís Otávio Z. Falsetti[1] | **René Delfos**[2] | **Florian Charruault**[3] | **Bruno Luchini**[3] | **Dirk Van Der Plas**[3] | **Victor C. Pandolfelli**[1]

[1]Materials Microstructure Engineering Group (GEMM), FIRE Associate Laboratory, Graduate Program in Materials Science and Engineering (PPGCEM), Federal University of Sao Carlos (UFSCar), São Carlos, São Paulo, Brazil

[2]Laboratory for Aero and Hydrodynamics, Delft University of Technology (TUDelft), Delft, The Netherlands

[3]Tata Steel Nederland, Velsen-Noord, The Netherlands

Correspondence
Luís Otávio Z. Falsetti, Materials Microstructure Engineering Group (GEMM), FIRE Associate Laboratory, Graduate Program in Materials Science and Engineering (PPGCEM), Federal University of Sao Carlos (UFSCar), Rod. Washington Luís (SP-310), km 235, Carlos, São Paulo, Brazil.
Email: luisotavio@dema.ufscar.br

Funding information
Fundação de Amparo à Pesquisa do Estado de São Paulo, Grant/Award Number: 2022/00378-2; Coordenação de Aperfeiçoamento de Pessoal de Nível Superior, Grant/Award Number: Finance Code 001

Abstract

Ceramic refractory bubbling devices may be applied in the steel ladle to induce the flotation of non-metallic inclusions to the slag phase. These inclusions have many origins along the steelmaking process and induce a detrimental effect on the mechanical properties of these metals. Therefore, the design of high-performance ceramic plugs relies on understanding the fundamentals of non-metallic inclusions captured by the gas bubbles. This study investigated the flotation dynamics of hydrophobic and hydrophilic hollow glass particles through experimentation using a water model and quantifying the particle concentration via light scattering. Both types of particles exhibited a comparable natural flotation removal rate, whereas a 40% increase for hydrophobic particles was observed when introducing 1.1 mm bubbles (at 25 NL/h) enhancing the efficiency from 43.1% to 65.2%. For hydrophilic particles, the efficiency increased from 59.1% to 86.2% when bubbles were injected into the system, whereas the removal rate decreased by 2.1-fold. The consequence of the practice of inert gas purging to remove non-metallic inclusions is also discussed.

KEYWORDS
interfaces, non-metallic inclusion, porous brick, refractory

1 | INTRODUCTION

The removal of non-metallic inclusions (NMI) is one of the targets for the secondary refining of steels and is conducted by injecting inert gases through porous bubblers either in the ladle or in the tundish. From a macroscopic point of view, the bubble plume interacts with the molten metal to capture inclusions, carrying them to the slag layer.[1,2] If properly adjusted (i.e., in chemical and rheological aspects), this top molten layer irreversibly dissolves the NMI, enhancing the cleanliness of the molten bath.[3] On the other hand, understanding the underlying microscopical mechanisms allows one to tune the process parameters and increase the removal rate and efficiency of the bubble-induced flotation which might also lead to the development of porous bubblers, also known as purging plugs.[4] In this sense, the literature describes three mechanisms by which inclusions interact with bubbles: (A) they

Notice that the paper was presented in part at a technical meeting—the Unified International Technical Conference on Refractories (UNITECR), in Frankfurt (Germany) from the 26th to the 29th of September 2023.

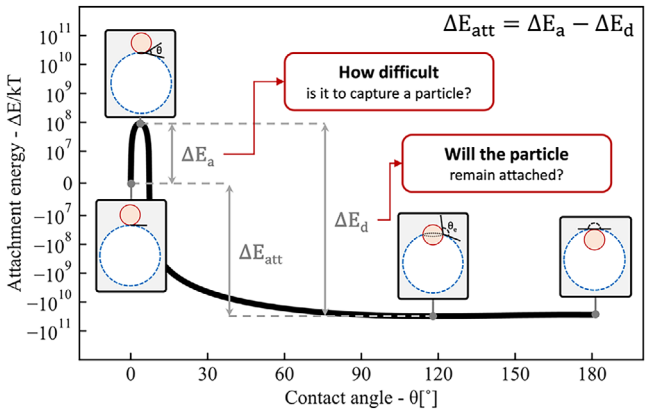

FIGURE 1 Typical energy curve for the attachment of particles with a contact angle of 115°.[8]

can be attached to the gas bubble's surface, (B) captured in the bubble wake region and (C) dragged by the flow pattern induced by the bubble plume.[5,6] It is worth noting that only mechanism "A" relies on a three-phase contact among the inclusion, gas bubble, and liquid medium. Thus, it may become relevant to investigate the interface tensions and their influence on the attachment step.[7]

The thermodynamics of particle attachment has been previously investigated by the authors in a former paper[8] that could be summarised as depicted in Figure 1. From the moment when the bubble-particle collision takes place, the three-phase contact line defines an angle for the particle on the bubble's surface (θ). By increasing this angle, the particle moves towards the bubble, facing an energy barrier to its attachment (ΔE_a). Thus, the magnitude of this energy barrier can be related to the easiness of capturing the inclusion. Once overcome, the system seeks a local minimum energy point, corresponding to the stable contact angle (θ_e). In some cases, typically for liquid-phobic inclusions, this point also corresponds to a global minimum, so the detachment of the inclusion back to the liquid phase is unlikely. For it to occur, the particle would need enough energy to overcome a detachment barrier (ΔE_d), which is higher than the attachment one (ΔE_a) when the latter represents a lowering in the system energy (i.e., $\Delta E_{att} < 0$). Conversely, the detachment barrier is lower than the attachment one for liquidphilic particles, as $\Delta E_{att} > 0$. Then, the particle could still be attached to the bubble surface, though in a metastable condition as it does not represent a global minimum energy point.[9]

Therefore, this work presents the design of experiments on a water model to assess the flotation of hydrophobic and hydrophilic particles, here playing the role of NMI. The particle concentration was measured timewise and the decay due to particle removal was exponentially fitted to get insights about the removal rate and process efficiency.

2 | EXPERIMENTAL PROCEDURES

Aiming at investigating the induced flotation of inclusions with different wettabilities, two grades of ceramic particles with similar size distributions were selected. Potters Q-Cel 7014 and 3M Glass Bubbles K-20 were deployed as hydrophobic and hydrophilic particles, respectively.[10,11] Both are spherical glass hollow spheres, with a density lower than the water one (0.14 and 0.20 g/cm^3, respectively). From the Stokes Law[12] (Equation (1)), the terminal velocity of a buoyant particle (v_t) is directly proportional to the square of the particle diameter (D_P). Also, it depends on the gravitational acceleration (g), the density of the solid (ρ_s) and the liquid (ρ_l), and the fluid's dynamic viscosity (η).

$$v_t = \frac{D_P^2\, g\, (\rho_s - \rho_l)}{18\, \eta} \quad (1)$$

Consequently, sieving the particles before the experiment is an alternative to lessen the natural flotation of particles, allowing the influence of bubble-induced flotation to be measured. Considering that the particle density is directly related to the ratio between its glass thickness layer and the hollow bulk, one could expect that smaller particles have a higher density, approaching the solid glass one. Therefore, the particles were dispersed on a 3:2 water-isopropanol solution and wet-sieved below 75 μm. The particles (as received) and the obtained suspensions were characterized in a Malvern Panalytical Mastersizer 2000 to get their size distribution, coupled with a Hydro 2000S sample dispersion unit. In these analyses, the solvent phase was ethanol 96% v/v for the hydrophobic particles and deionized water for the hydrophilic ones. All samples were analyzed according to Fraunhofer's theory of light scattering.[13] Scanning electron microscopy micrographs were obtained by a TESCAN MIRA microscope under high vacuum, using the secondary electron mode with an acceleration voltage of 25 kV, a working distance of 15 mm, and a beam current of 300 pA. Samples were coated with a 10 nm layer of AuPd alloy.

The water model comprised a 1000 × 400 × 40 mm^3 vessel with acrylic walls to allow the visualisation of the experiments, as illustrated in Figure 2A. The system is filled in with softened tap water and has a pump to recirculate the aqueous suspension and homogenise the concentration of particles. During the experiments, the pump is kept at 900 rpm, corresponding to a recirculating flow of 21 L/min or a velocity of roughly 22 mm/s when considering the model's cross-section. A porous bubbler was installed at the centre of the model's base, where compressed air was blown to generate bubbles close to 1.1 mm

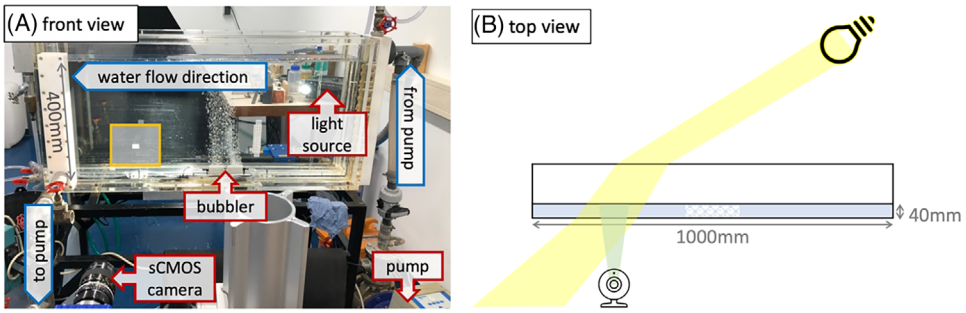

FIGURE 2 Water model's (A) front view—highlighting the recirculation path (in blue), the various apparatus (in red), and the field of view (in yellow)—and (B) top view—illustrating the light scattering system.

(90% of bubbles in the range of 0.7–1.5 mm). In the current experiments, the water model was applied to investigate the interaction between particles and bubbles from a fundamental point-of-view, not aiming to reproduce any kind of steel vessel, yet. However, some similarities to tundishes operating with bubble curtains might be seen considering the crossflow between the ascending bubble plume and the recirculating particle-containing liquid. When compared to the ladle, where purging plugs are typically installed, a few similarities could be pointed out.

The concentration of particles was indirectly measured by a light scattering technique, as represented in Figure 2B. A 250-watt tungsten-halogen lamp, located in the back part of the model, was used as a source of collimated light. The light rays are scattered by the particle and collected by a sCMOS camera (LaVision Imager) in front of the model, at 1 Hz. The camera has a Nikon 55 mm lens installed at full aperture (f/2.8). Each frame has 2160 × 2560 pixels, is 16-bit deep and corresponds to a 1 ms exposure time. The advantage of this inline technique is the continuous measurement of particle concentration by averaging the light intensity over an area (highlighted in yellow in Figure 2A).

Before starting the experiments, 80 mL of particle suspension was injected close to the water outflow and the model was homogenised for 5 min. Then, the natural flotation of particles was recorded for 10 min and fitted by an exponential decay function ($I(t) = I_\delta \cdot \exp(TS^{-1} \cdot t) + I_\infty$), where TS stands for "time scale" and represents the mean lifetime of particles in suspension.[14] Next, compressed air was injected through a porous bubbler and the induced flotation of particles was recorded for 25 min, and mathematically adjusted. As the floated particles remain on the model's top surface, the lowest gas flow rate allowed by the experimental setup was chosen (25 NL/h) and the outcomes are discussed in this work based on the particle's wettability. Finally, particles were filtered out and the system's background with bubbles was measured.

The system had been previously investigated in terms of repeatability, when a similar flotation experiment was conducted and yielded a coefficient of variation of 10% and 6.8% for the removal efficiency and the time scale, respectively. It has been calibrated within the analyzed range (700–9000 counts), showing a linear correlation to the particle concentration. Thus, after fitting the intensity curve by the exponential decay, the initial value ($I_{t=0}$) is taken as the 0% of removed particles and the background measurement as the 100%, so that the intensity recorded by the sCMOS camera may be converted into particle concentration in percentage.

3 | RESULTS AND DISCUSSIONS

3.1 | Suspension characterization

As this work aims to compare the share of the bubble plume to the induced mechanisms of particle flotation based on its wettability, it is crucial to isolate the variable by keeping the others as constants (for instance, the particle size and distribution). Thus, the first results are related to the characterization of the particle suspensions to assert that hydrophilic and hydrophobic particle grades have similar granulometry. The particle grades were characterized by their size distribution before and after the wet-sieving procedure, resulting in a suspension of fine particles. The results of size distribution are presented in Figure 3, based on which one can notice the similarity in size distribution between the hydrophilic and hydrophobic grades. It is also possible to infer that the sieving procedure not merely removed particles above 75 μm but generated a new distribution of smaller particles. For the hydrophilic grade, the values of d_{10}, d_{50}, and d_{90} (see Table 1) were cut down to two-thirds whereas these values decreased by roughly half for the hydrophobic one.

The particles and their suspensions were also analyzed by electron microscopy and the micrographs are presented in Figure 4A–D. The images show that the particles are perfectly round, and few fragments and debris are observed in

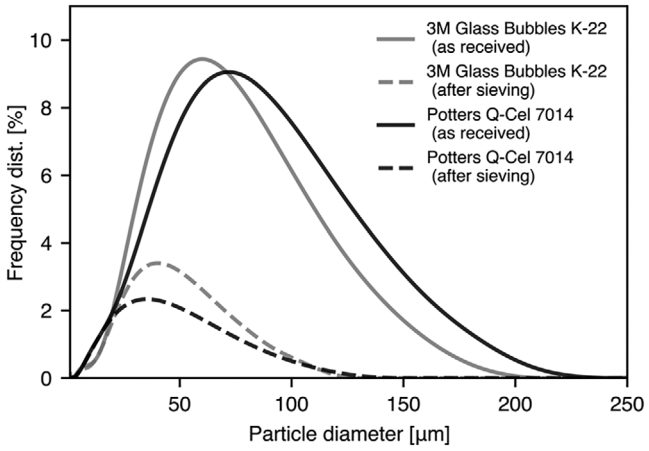

FIGURE 3 Particle size distribution obtained by a Malvern analyzer before and after the wet-sieving procedure.

TABLE 1 Particle diameters measured from their size distribution before and after the wet-sieving procedure.

Sample		d_{10} [μm]	d_{50} [μm]	d_{90} [μm]
As received	3M K-20	21.6	51.1	100
	Potters 7014	20.2	57.6	114
In suspension	3M K-20	14.2	34.2	66.1
	Potters 7014	10.1	28.5	64.3

the samples before sieving. There is a noticeable decrease in average particle size after wet-sieving and preparing the suspensions, which attests to the results in Figure 3. However, small fragments of broken particles were also among the sieved fraction that was suspended, and the debris would tend to sediment during the experiments.

3.2 | Flotation experiments of hydrophobic and hydrophilic particles

The sieved suspension of hydrophobic particles was used in the flotation experiment and the results are shown in Figure 5, which presents the percentage of removed particles as a function of time. The first increase of particle removal represents the particles' natural flotation as no gas bubbles were being injected into the system, and the exponential fitting (dashed red line) shows that the particle concentration tends to an efficiency of 43.1% at an infinite time. After 10 min, bubbles started to be injected into the system, leading to an instantaneous increase in light scattering due to the presence of tiny bubbles in the camera's field of view, which tend to float straightaway. Then, the flotation speeded up as the TS (time scale) parameter was reduced from 663 to 474 s (i.e., a 40% faster removal), and the efficiency increased to 65.2% (1.63 times the one for plain natural flotation) as the mechanisms of induced flotation were coupled by the bubble plume.

The experiment with hydrophobic particles highlighted the higher removal rate and efficiency when bubbles were injected. However, the three mechanisms of bubble-induced flotation are simultaneously contributing to this result, making it impossible to determine their share. Thus, the same experiment was carried out with the sieved suspension of hydrophilic particles and the results are presented in Figure 6. During the natural flotation step, the exponential fitting led to a TS parameter of 727 s and an efficiency of 59.1%. Conversely, to the previous experiment, the injection of bubbles initially led to a slight increase in the scattered light, as indicated by the decrease of particle removal in Figure 6. This effect might be related to the re-entrainment of particles from the top surface of the system as the bubble plume locally increases the instability of this layer. After 6 min, the removal and the re-entrainment of particles came to a stable condition and the results were fitted by an exponential equation. Although the removal rate decreased 2.1-fold, with TS moving from 727 to 2264 s, the efficiency increased to 86.2% (1.46 times the natural flotation's one) when induced flotation mechanisms were coupled.

Based on the results, the injection of gas increased the removal efficiency regardless of the particle wettability. From the mechanisms of induced flotation, one could expect a higher efficiency increase for the hydrophobic particles when compared to the hydrophilic ones as the attachment to the bubble surface is unlikely to occur. Besides, the removal rate speeded up in the experiment of non-wettable particles, indicating that bubble injection is advisable to start as soon as possible during the liquid metal refining step. On the other hand, the induced flotation of wettable particles increased the efficiency while decreasing the removal rate, showing that too early gas purging in the process could lead to a delay in the removal of non-metallic inclusions.

Regarding the re-entrainment of hydrophilic particles when the bubble plume was started, the instability of the floated particles layer at the water model's top region may be related to the thermodynamics of capturing particles at liquid-gas interfaces. As shown in Figure 7, the change in energy due to the attachment depends on the macroscopic contact angle (θ_{slg}) among the solid, liquid, and gas phases, defining three scenarios:

(i) Non-wettable particles (90° or higher) show a negative ΔE_{att}, causing the detachment barrier to be higher than the attachment one ($\Delta E_a < \Delta E_d$). Thus, particles are stable at the liquid-gas interface, as in the experiment with hydrophobic particles (Figure 5);

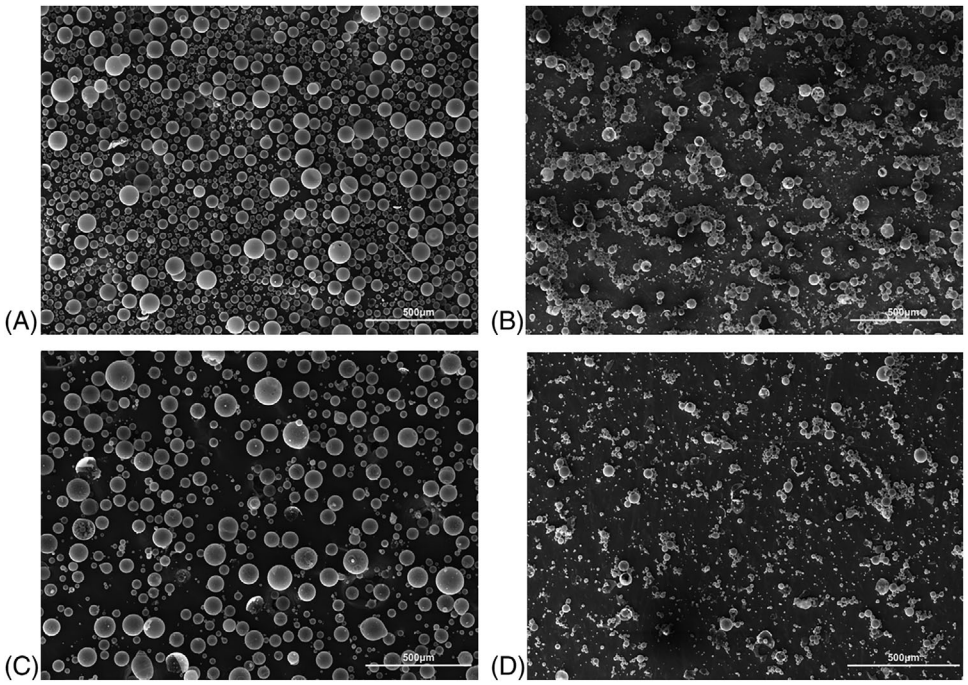

FIGURE 4 Micrographs of (A,B) hydrophilic and (C,D) hydrophobic particles, before and after wet-sieving, respectively.

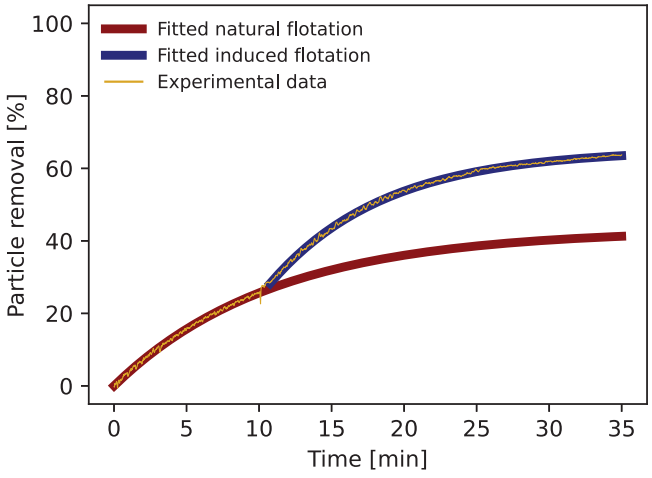

FIGURE 5 Particle removal as a function of time for the flotation experiment with hydrophobic particles.

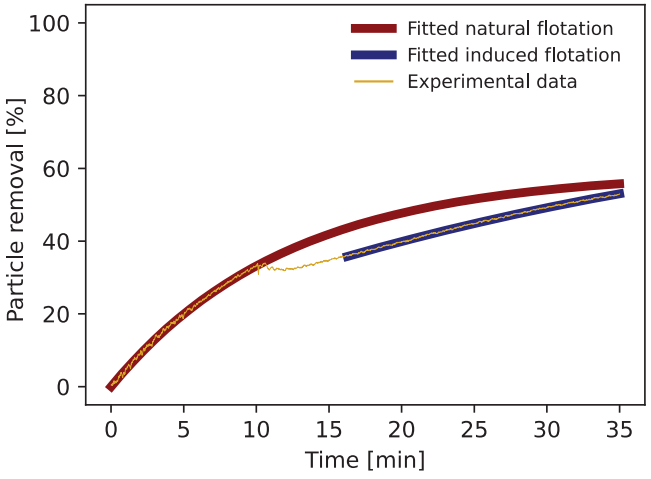

FIGURE 6 Intensity of scattered light as a function of time for the flotation experiment with hydrophilic particles, highlighting the particle re-entrainment after bubble injection starts.

(ii) Slightly wettable particles (around 60°) can still be attached to the liquid-gas interface because a local minimum energy point is observed beyond the attachment barrier. However, it represents a metastable condition as ΔE_{att} is positive (and $\Delta E_d < \Delta E_a$), causing the particle to detach and return to the liquid phase easily;

(iii) Highly wettable particles (30° or lower) do not even have a metastable condition of attachment, and the energy components (ΔE_{att}, ΔE_d, and ΔE_a) are not applicable.

Considering that the hydrophilic grade of particles (3M Glass Bubbles K-20) was made of soda-lime-borosilicate glass with no surface treatment to change their hydrophilicity, one could expect a low macroscopic wetting angle in contact with aqueous solutions and, therefore, a condition close to the third scenario—where particles are not stable at the liquid-gas interface. Thus, the naturally floated particles remained at the model's top surface merely because of their low density (compared to the water phase) and re-entrained the system when the bubble plume started, increasing the

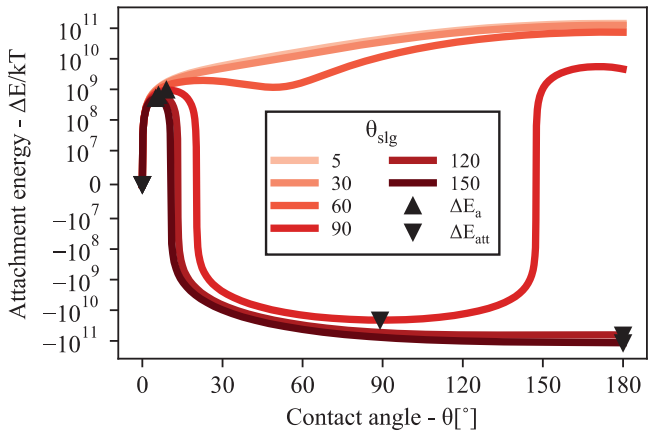

FIGURE 7 Change in energy caused due to the attachment of a particle at a liquid-gas interface as a function of its position for different values of macroscopic contact angles (θ_{slg}). Obtained as described[8] considering hypothetical values of liquid-gas tension ($\gamma_{lg} = 72.8 mJ/m^2$), line tension ($\gamma_{slg} = 0.3 \mu J/m^2$), bubble size ($D_B = 1$ mm), particle size ($D_P = 50$ μm) and contact angle (θ_{slg}).

turbulence of the top layer. On the other hand, the additional flotation mechanisms—related to either the particles captured by the bubble wake region or by the induced flow pattern—would still be activated, which explains the higher efficiency of removal when bubbles were injected (Figure 6). Therefore, changes in the system to remove the floated hydrophilic particles right after reaching the top layer would be required for future experiments so that it can suitably act as a slag layer.[15]

4 | CONCLUSIONS

This work analyzed the flotation behavior of hydrophobic and hydrophilic hollow glass particles by conducting experiments on a water model and measuring the particle concentration by a light scattering technique. Particles were pre-dispersed in an isopropanol-water solution and wet-sieved to generate inclusion-like suspensions. The natural flotation of both particles presented a similar removal rate. When 1.1 mm bubbles were injected, the removal rate for hydrophobic particles increased by 40%, and the removal efficiency was 1.63 times the natural flotation's efficiency. Conversely, the bubble plume caused a decrease of 2.1-fold in the removal rate of hydrophobic particles, although the efficiency was 1.46 times the natural flotation one. During this latter experiment, the naturally floated hydrophilic particles re-entrained from the model's top region as bubbles were injected. Such an effect was expected as these particles are highly wet by the liquid and not captured by the liquid-gas interface due to their low contact angle.

ACKNOWLEDGMENTS

This study was financed in part by the Coordenação de Aperfeiçoamento de Pessoal de Nível Superior—Brasil (CAPES)—Finance Code 001 and by the São Paulo Research Foundation (FAPESP)—grant 2022/00378-2. The authors are also thankful to Dr Dereck N. Ferreira Muche for the technical discussions, to MSc Otávio H. Borges and Laboratory of Structural Characterization (LCE/DEMa/UFSCar) for the micrographs, and to FIRE (Federation for International Refractory Research and Education) for supporting this research.

ORCID

Luís Otávio Z. Falsetti https://orcid.org/0000-0002-2476-692X
René Delfos https://orcid.org/0000-0002-9693-2245
Florian Charruault https://orcid.org/0000-0002-6936-3032
Bruno Luchini https://orcid.org/0000-0002-5940-5163
Victor C. Pandolfelli https://orcid.org/0000-0002-1711-9804

REFERENCES

1. Zhang L, Taniguchi S. Fundamentals of inclusion removal from liquid steel by bubble flotation. Int Mater Rev. 2000;45(2):59–82. https://doi.org/10.1179/095066000101528313
2. Zhang L, Aoki J, Thomas BG. Inclusion removal by bubble flotation in a continuous casting mold. Metall Mater Trans B. 2006;37(3):361–79. link.springer.com/10.1007/s11663-006-0021-z
3. Ren Y, Zhu P, Ren C, Liu N, Zhang L. Dissolution of SiO_2 inclusions in CaO-SiO_2-based slags in situ observed using high-temperature confocal scanning laser microscopy. Metall Mater Trans B. 2022;53(2):682–92. https://doi.org/10.1007/s11663-021-02401-5
4. Falsetti LOZ, Ferreira Muche DN, Andreeta MRB, Moreira MH, Pandolfelli VC. Bubble generation in refractory porous plugs: The role of the ceramic surface composition. Int J Ceram Eng Sci. 2022;4(3):199–210. https://doi.org/10.1002/ces2.10132
5. Zheng S, Zhu M. Physical modelling of inclusion behaviour in secondary refining with argon blowing. Steel Res Int. 2008;79(9):685–90. https://doi.org/10.2374/SRI07SP134-79-2008-685
6. Yang HL, He P, Zhai YC. Removal behavior of inclusions in molten steel by bubble wake flow based on water model experiment. ISIJ Int. 2014;54(3):578–81. https://doi.org/10.2355/isijinternational.54.578
7. Scheludko A, Toshev B V., Bojadjiev DT. Attachment of particles to a liquid surface (capillary theory of flotation). J Chem Soc Faraday Transl Phys Chem Condens Phases. 1976;72:2815–28. https://doi.org/10.1039/F19767202815
8. Falsetti LOZ, Ferreira Muche DN, Santos Junior T dos, Pandolfelli VC. Thermodynamics of smart bubbles: The role of interfacial energies in porous ceramic production and non-metallic inclusion removal. Ceram Int. 2021;47(10PA):14216–25. https://doi.org/10.1016/j.ceramint.2021.02.006

9. Law BM, McBride SP, Wang JY, Wi HS, Paneru G, Betelu S, et al. Line tension and its influence on droplets and particles at surfaces. Prog Surf Sci. 2017;92(1):1–39. https://doi.org/10.1016/j.progsurf.2016.12.002
10. Potters Europe engineered glass materials division—technical report. 2003 https://docplayer.net/docview/68/59761748/
11. 3M. Glass Bubbles K Series—product information. 2013. https://www.3m.com/3M/en_US/p/d/b40064606/
12. Spasic AM. Chapter 1 - Introduction in: A.M.B.T.-I.S., Spasic T, editors. Rheology of emulsions. Amsterdam, NL: Elsevier; 2018: pp. 1–25. https://doi.org/10.1016/B978-0-12-813836-6.00001-5
13. Foerter-Barth U, Teipel U. Characterization of particles by means of laser light diffraction and dynamic light scattering. Dev Miner Proc. 2000;13:C1–1–C1–8. https://doi.org/10.1016/S0167-4528(00)80003-4
14. Gharai M, Venugopal R. Modeling of flotation process—an overview of different approaches. Miner Process Extr Metall Rev. 2016 [cited 2023 Jan 17];37(2):120–33. https://doi.org/10.1080/08827508.2015.1115991
15. Zhang MJ, Gu HZ, Huang A, Zhu HX, Deng CJ. Physical and mathematical modeling of inclusion removal with gas bottom-blowing in continuous casting tundish. J Min Metall Sect B Metall. 2011;47(1):37–44. https://doi.org/10.2298/JMMB1101037Z

How to cite this article: Falsetti LOZ, Delfos R, Charruault F, Luchini B, Van Der Plas D, Pandolfelli VC. Wettability of non-metallic inclusions and its impact on bubble-induced flotation kinetics. Int J Appl Ceram Technol. 2024;21:3835–41. https://doi.org/10.1111/ijac.14849